

# Geophysical Research Letters

## RESEARCH LETTER

10.1002/2017GL073475

### Key Points:

- South Pacific atmospheric variability, namely, the South Pacific Oscillation (SPO), plays a key role in the prediction of ENSO flavors
- The sources of variability of the SPO are both intrinsic and also forced by anomalous convection in the central tropical Pacific
- The SPO potentially plays a significant role in climate variability on multiple timescales: seasonal, interannual, and multidecadal

### Supporting Information:

- Supporting Information S1

### Correspondence to:

Y. You,  
Yujia.You-1@ou.edu

### Citation:

You, Y. and J. C. Furtado (2017),  
The role of South Pacific atmospheric  
variability in the development of  
different types of ENSO, *Geophys. Res.  
Lett.*, 44, doi:10.1002/2017GL073475.

Received 16 MAR 2017

Accepted 28 JUN 2017

Accepted article online 5 JUL 2017

## The role of South Pacific atmospheric variability in the development of different types of ENSO

Yujia You<sup>1</sup>  and Jason C. Furtado<sup>1</sup> 

<sup>1</sup>School of Meteorology, University of Oklahoma, Norman, Oklahoma, USA

**Abstract** Recent advances in tropical Pacific climate variability have focused on understanding the development of El Niño–Southern Oscillation (ENSO) events, specifically the types or “flavors” of ENSO (i.e., central versus eastern Pacific events). While precursors to ENSO events exist, distinguishing the particular flavor of the expected ENSO event remains unresolved. This study offers a new look at ENSO predictability using South Pacific atmospheric variability during austral winter as an indicator. The positive phase of the leading mode of South Pacific sea level pressure variability, which we term the South Pacific Oscillation (SPO), exhibits a meridional dipole with a(n) (anti)cyclonic anomaly dominating the subtropics (extratropics/high latitudes). Once energized, the cyclonic anomalies in the subtropical node of the SPO weaken the southeasterly trade winds and promote the charging of the eastern equatorial Pacific Ocean, giving rise to eastern Pacific ENSO events. Indeed, the type of ENSO event can be determined accurately using only the magnitude and phase of the SPO during austral winter as a predictor (17 out of 23 cases). The SPO may also play a role in explaining the asymmetry of warm and cold events. Collectively, our findings present a new perspective on ENSO–South Pacific interactions that can advance overall understanding of the ENSO system and enhance its predictability across multiple timescales.

### 1. Introduction

The El Niño–Southern Oscillation (ENSO) is one of the most prominent year-to-year fluctuation in the Earth climate system and influences tropical convective processes along with the global atmospheric circulation. In recent decades, increasing interests have been placed on the diversity of ENSO events—i.e., eastern Pacific (EP) versus central Pacific (CP) El Niño events [Ashok *et al.*, 2007; Yu *et al.*, 2012]—due to their distinct remote impacts. For CP events, the sea surface temperature anomaly (SSTA) extends from Baja California southwestward to the central equatorial Pacific and thereafter remains and amplifies in situ [Kao and Yu, 2009; Kug *et al.*, 2009; Yu *et al.*, 2010; Capotondi *et al.*, 2015]. The evolution of EP events features rapid warming of SSTs over the eastern tropical Pacific [e.g., Wyrtki, 1975; Rasmusson and Carpenter, 1982] explained by theories like the delayed oscillator [e.g., Suarez and Schopf, 1988] and the discharge-recharge mechanisms [e.g., Jin, 1997]. The two types of ENSO events may be distinguishable, although some studies suggest that ENSO flavors come in a nondiscrete continuum [e.g., Johnson, 2013; Karnauskas, 2013].

Aside from the mechanisms of formation, research on the precursors to specific ENSO events has also been conducted. Particularly, the presence of the North Pacific Oscillation (NPO), characterized by a large-scale meridional sea level pressure (SLP) anomaly (SLPa) dipole between roughly Alaska and Hawaii [e.g., Rogers, 1981; Linkin and Nigam, 2008], serves as an important precursor for ENSO ~9 months before the event [Chang *et al.*, 2007]. Dynamically, the anomalous circulations associated with the southern node of the NPO modulate the off-equatorial trade winds, charge the central equatorial heat content [Anderson *et al.*, 2013a; Anderson and Perez, 2015], and may initiate an ENSO event [e.g., Vimont *et al.*, 2003; Chiang and Vimont, 2004]. However, there is little evidence currently that the NPO precursor favors one type of ENSO over the other [e.g., Ding *et al.*, 2015; Di Lorenzo *et al.*, 2015], although it may influence the longitude of the warmest SSTa [Anderson *et al.*, 2013b]. Turning to the Southern Hemisphere, Zhang *et al.* [2014] argue for the importance of the South Pacific Meridional Mode (SPMM) in initiating EP ENSO events, although the origin of the SPMM is unclear. Extratropical South Pacific ocean dynamics may also play an important role in extended predictability of ENSO events, with off-equatorial wind stresses impacting tropical Pacific thermocline depths

[McGregor *et al.*, 2009a, 2009b]. Debate on cause and effect between South Pacific atmospheric variability and ENSO remains an open research question [e.g., Jin and Kirtman, 2009].

The present study examines the linkages between the extratropical South Pacific atmosphere and tropical Pacific SST variations associated with different types of ENSO. Our findings indicate that a prominent mode of South Pacific atmospheric variability is likely a favorable condition for the formation of EP versus CP ENSO events. Thus, this work can be viewed as a stepping stone to recognize the importance that the South Pacific plays in generation of ENSO events, mirroring (and adding to) existing results of the role of North Pacific atmospheric variability on tropical Pacific climate variability.

## 2. Data and Methods

Monthly mean atmospheric fields (SLP, 10 m winds) from the National Centers for Environmental Prediction/National Center for Atmospheric Research (NCEP/NCAR) reanalysis 1 [Kalnay *et al.*, 1996] from 1948 to 2015 are employed in this study. SST and subsurface ocean data over the same period are taken from the Hadley Centre Global Sea Ice and Sea Surface Temperature data set [Rayner *et al.*, 2003] and the Ocean Reanalysis System 4 European Centre for Medium-Range Weather Forecasts (ECMWF) ocean analysis [Balmaseda *et al.*, 2013]. Anomalies of all fields are derived by subtracting the long-term climatology (1981–2010) for a particular month from the monthly mean values. All data are linearly detrended, and a 3 month running mean is applied before statistical analyses are conducted.

Several climate indices are derived and used in this study. The cold tongue index (CTI; SSTa averaged over 6°S–6°N, 180°W–90°W), the Niño-3 (5°S–5°N, 150°W–90°W), and the Niño-4 (5°S–5°N, 160°E–150°W) indices are used to represent ENSO variability. An El Niño (A La Niña) is defined as a year in which the December–February (DJF) Niño-3 index or Niño-4 index exceeds (is lower than) 0.5°C (−0.5°C). An EP (CP) ENSO event is then classified using the same criterion as Yeh *et al.* [2009]: i.e., an ENSO event during which the DJF Niño-3 index is greater (less) than the DJF Niño-4 index.

Linear regression, compositing, and empirical orthogonal function (EOF) analyses are the primary statistical tools used in this study. For some analyses, we are interested in removing the linear dependence of a time series  $y(t)$  with some other climate mode or variable  $x(t)$  to examine residual variability. Calling this residual,  $y_{-rx}$ :  $y_{-rx}(t) = y(t) - [\alpha + \beta \times x(t)]$ , where  $\alpha$  and  $\beta$  are found through least squares fitting. Thus,  $y_{-rx}(t)$  is, by definition, uncorrelated with  $x(t)$ . Statistical significance of regression coefficients is determined by a two-tailed Student's  $t$  test with an effective degrees of freedom  $N^*$  computed in Bretherton *et al.* [1999] as follows:

$$N^* = N \frac{1 - r_1 r_2}{1 + r_1 r_2} \quad (1)$$

where  $N$  is the total sample size and  $r_1$  and  $r_2$  are the lag 1 correlations of the index and field used in the particular analysis, respectively.

Finally, in investigating oceanic pathways linking the South Pacific to the tropical Pacific, we compute the depth-integrated meridional velocity  $V$  (i.e., Sverdrup transport) as in Anderson and Perez [2015]

$$V \approx \frac{1}{\beta \rho} \left[ \frac{\partial \tau_y}{\partial x} - \frac{\partial \tau_x}{\partial y} \right] \quad (2)$$

where  $\tau_x$  and  $\tau_y$  are the eastward and northward components of the wind stress, respectively,  $\beta$  is the latitudinal gradient of the Coriolis parameter, and  $\rho = 1025 \text{ kg/m}^3$  is the density of sea water. The wind stresses are computed as  $\tau = C_D \rho_{\text{air}} U^2$ , where  $C_D = 0.0013$  is the drag coefficient,  $\rho_{\text{air}} = 1.2 \text{ kg/m}^3$  is the density of air, and  $U$  is the 10 m wind speed.

## 3. Results

### 3.1. The Leading Mode of South Pacific Atmospheric Variability

We begin by examining the dominant modes of South Pacific atmospheric variability via EOF analysis of monthly mean South Pacific SLPa field over the domain 10°S–45°S, 160°W–70°W. Figure 1a shows the regression of monthly SLPa (line contours), SSTa (shading), and 10 m wind anomalies (vectors) onto the standardized leading principal component (PC1) time series of monthly mean South Pacific SLPa. The leading mode explains

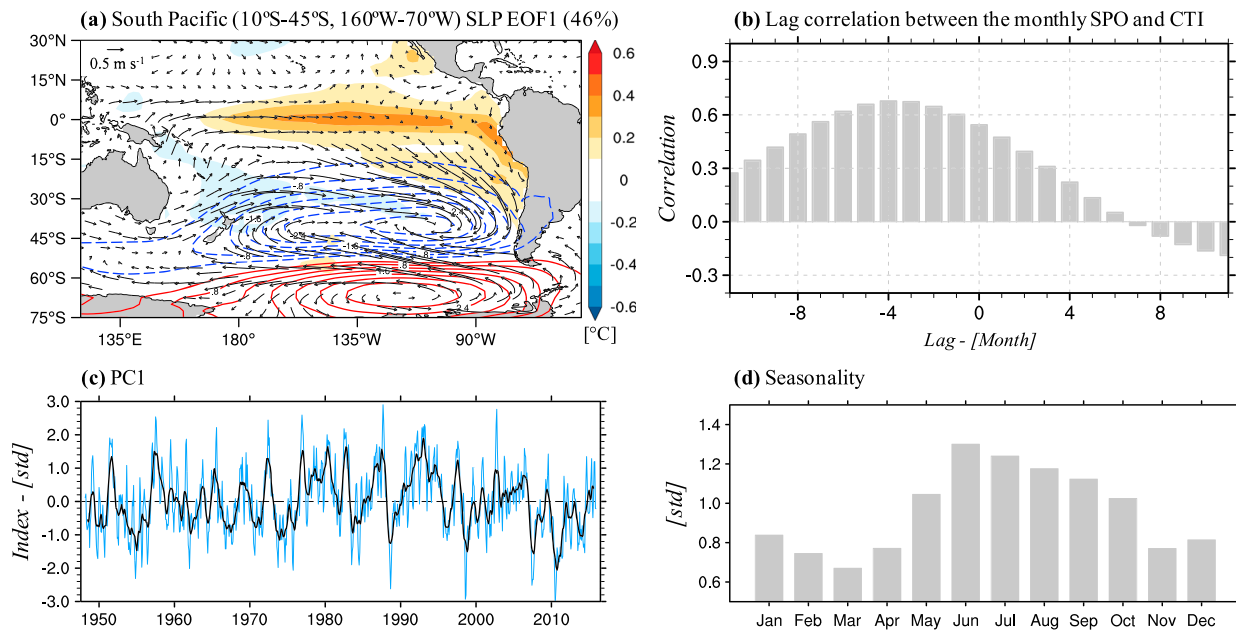


**Figure 1.** (a) Regression of SLPa (contour, hPa), SSTa (shading,  $^{\circ}\text{C}$ ), and 10 m wind anomalies (vector,  $\text{m s}^{-1}$ ) onto the standardized PC1 time series of monthly mean South Pacific SLPa (i.e., the SPO index). Contour interval 0.4 hPa (line contours) and  $0.1^{\circ}\text{C}$  (shading). Reference wind vector  $0.5 \text{ m s}^{-1}$ . Solid (dashed) line contours indicate positive (negative) values. Zero contour omitted. (b) The lag correlation between the SPO index and the CTI. Negative (positive) lags indicate that the SPO index leads (lags) the CTI. (c) The standardized SPO index (blue) and its 9 month running mean (black). (d) Seasonality of the SPO index expressed by the standard deviation as a function of calendar month.

about 46% of the total variance in South Pacific SLPa, is significantly separated from higher-order modes per North *et al.* [1982] criterion, and is robust to reasonable variations in the domain size (not shown). The positive phase features a SLPa dipole between the subtropics (cyclonic anomalies) and middle to high latitudes (anticyclonic anomalies) with an equivalent barotropic structure throughout the troposphere (not shown). For this study, we call this SLPa pattern the South Pacific Oscillation (SPO), owing to its analogous structure to the NPO and its associated time series (i.e., PC1) the SPO index. The cyclonic SLPa generally overlaps the location of the South Pacific High and thus weakens the climatological southeasterly trade winds (Figure 1a, vectors). The positive phase of the SPO also covaries strongly with warm SSTa throughout the central and eastern tropical Pacific (Figure 1a, shading). Indeed, the SPO is significantly correlated with the CTI ( $r = 0.56$ ;  $p < 0.01$ ) with the maximum correlation occurring when the SPO leads the CTI by 3–4 months (Figure 1b), consistent with other works [e.g., Jin and Kirtman, 2009]. SPO variability spans a wide range of time scales (intraseasonal, interannual, and even decadal; Figure 1c) with seasonal variability maximized during austral winter (i.e., June–August, JJA; Figure 1d).

### 3.2. Variability of the SPO and Links to the Tropical Pacific

To elucidate the connections between the SPO and the tropical Pacific, we focus on the austral winter (JJA) when the SPO is most variable. Figure 2 shows the lagged-regression maps of SLPa, SSTa, and 10 m wind anomalies onto the standardized JJA SPO ( $\text{SPO}_{\text{JJA}}$ ) index from March–May (MAM) through DJF + 1 (i.e., the peak season for ENSO). During MAM (Figure 2a), the characteristic SSTa and wind anomaly patterns associated with the NPO/NPMM are apparent [e.g., Chiang and Vimont, 2004]. By JJA, a canonical (i.e., EP) El Niño is established with the maximum SSTa over the central and eastern tropical Pacific (Figure 2b, shading) concomitant with a positive SPO (Figure 2, line contours). From JJA to September–November (SON), the anomalous wind stresses associated with the SPO promote anomalous equatorial divergence of water west of  $150^{\circ}\text{W}$  in both hemispheres, as shown by the regression of  $V$  onto the  $\text{SPO}_{\text{JJA}}$  index (Figures 2f and 2g). By contrast, anomalous equatorward mass transport is centered south of the equator between  $150^{\circ}\text{W}$ – $90^{\circ}\text{W}$  (Figures 2f and 2g), colocated with the warmest SSTa (Figures 2b and 2c), thereby charging the eastern equatorial Pacific in accordance with the “trade wind charging” mechanism [Anderson *et al.*, 2013a; Anderson and Perez, 2015]. Hence, positive ocean heat content builds in the central tropical Pacific and eventually discharges to the east from JJA to DJF (Figures 2f and 2g), resulting in a warm EP ENSO event (Figure 2d).

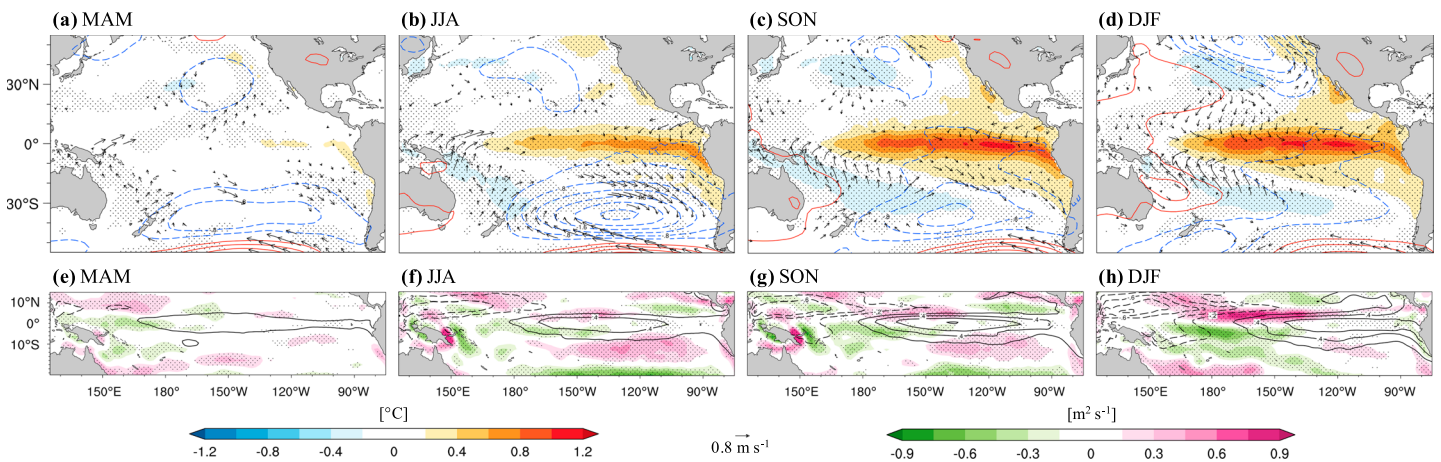


**Figure 2.** Lag regression of SLPa (contours, hPa), SSTa (shading, °C), and 10 m wind anomalies (vector, m s<sup>-1</sup>) onto the standardized SPO<sub>JJA</sub> index for (a) March–May (MAM), (b) June–August (JJA), (c) September–November (SON), and (d) December–February (DJF). For Figure 2a, the fields lead the SPO<sub>JJA</sub> index, while for Figures 2c and 2d, the SPO<sub>JJA</sub> index leads the fields. Contour interval 0.2°C for SSTa and 0.4 hPa for SLPa. Reference wind vector 0.8 m s<sup>-1</sup>. Wind vectors plotted only where significant at the  $p < 0.05$  level. (e–h) As in Figures 2a–2d except for the anomalous vertically integrated meridional oceanic mass transport ( $V$ ; shading, m<sup>2</sup> s<sup>-1</sup>) and ocean heat content (vertically averaged temperature integrated from 0 to 300 m; contour, °C). Contour interval 0.15 m<sup>2</sup> s<sup>-1</sup> for  $V$  and 0.2°C for ocean heat content. Solid (dashed) line contours indicate positive (negative) values. Zero contour omitted. Stippling indicates statistically significant SSTa regression coefficients at the  $p < 0.05$  level according to a two-tailed Student's  $t$  test.

Is the SPO merely a response to tropical Pacific forcing? or does it contain significant internal variability that can impact tropical Pacific SSTa? To answer this question, Figure 3a shows the regression of JJA SLPa (contours), SSTa (shading), and 10 m wind anomalies (vectors) onto the CTI<sub>JJA</sub> index. The SLPa field clearly displays a SPO-like structure in the South Pacific, indicating that at least a portion of its variability covaries with tropical Pacific SSTa. Next, to examine the potential stochastic component of the SPO, we conduct EOF analysis on the *residual* South Pacific SLPa field, i.e., the SLPa field after linearly removing the CTI<sub>JJA</sub> index:  $\text{SLPa}_{\text{res}} = \text{SLPa} - [\alpha + \beta \times \text{CTI}_{\text{JJA}}]$ . Therefore,  $\text{SLPa}_{\text{res}}$  has exactly zero correlation with tropical Pacific SSTa. The leading mode of  $\text{SLPa}_{\text{res}}$  (i.e., the spatial pattern EOF1<sub>res</sub> and its associated time series PC1<sub>res</sub>) accounts for 48% of the variance in  $\text{SLPa}_{\text{res}}$  and resembles strongly the SPO (Figure 3b, line contours;  $r = 0.79$  ( $p < 0.01$ ) between SPO<sub>JJA</sub> and PC1<sub>res</sub> indices). Therefore, we find that the SPO cannot be viewed only as a response to tropical Pacific SSTa but instead contains significant (and independent) internal variability that can play a role in the development of an ENSO event.

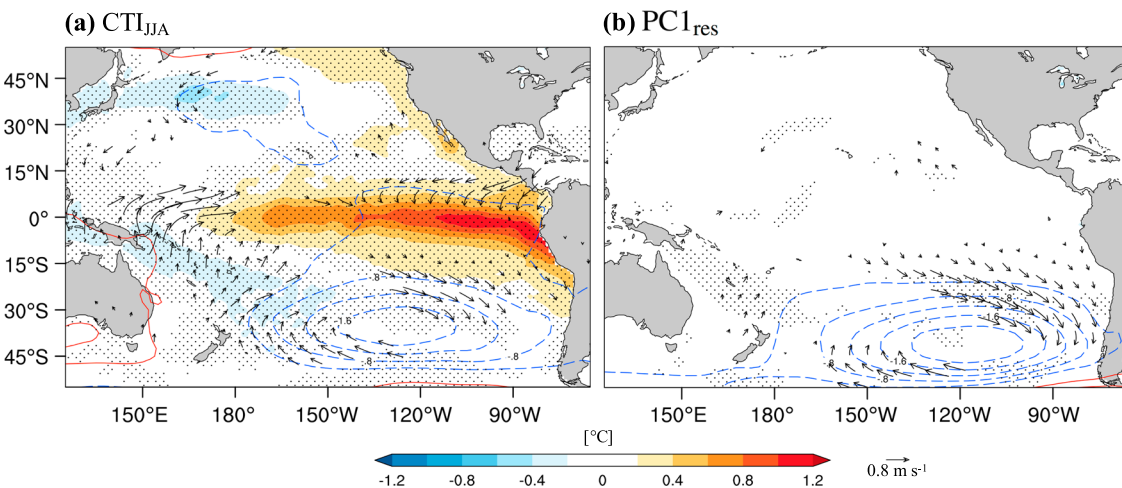


**Figure 3.** (a) Regression of June–August (JJA) SLPa (contour, hPa), SSTa (shading, °C), and 10 m wind anomalies (vector, m s<sup>-1</sup>) onto the standardized CTI index. (b) As in Figure 3a, except for regression onto the standardized PC1<sub>res</sub> index (see text for details). Contour interval 0.2°C for SSTa and 0.4 hPa for SLPa. Reference wind vector 0.8 m s<sup>-1</sup>. Solid (dashed) line contours indicate positive (negative) values. Zero contour omitted. Wind vectors plotted only where significant at the  $p < 0.05$  level. Stippling as in Figure 2.

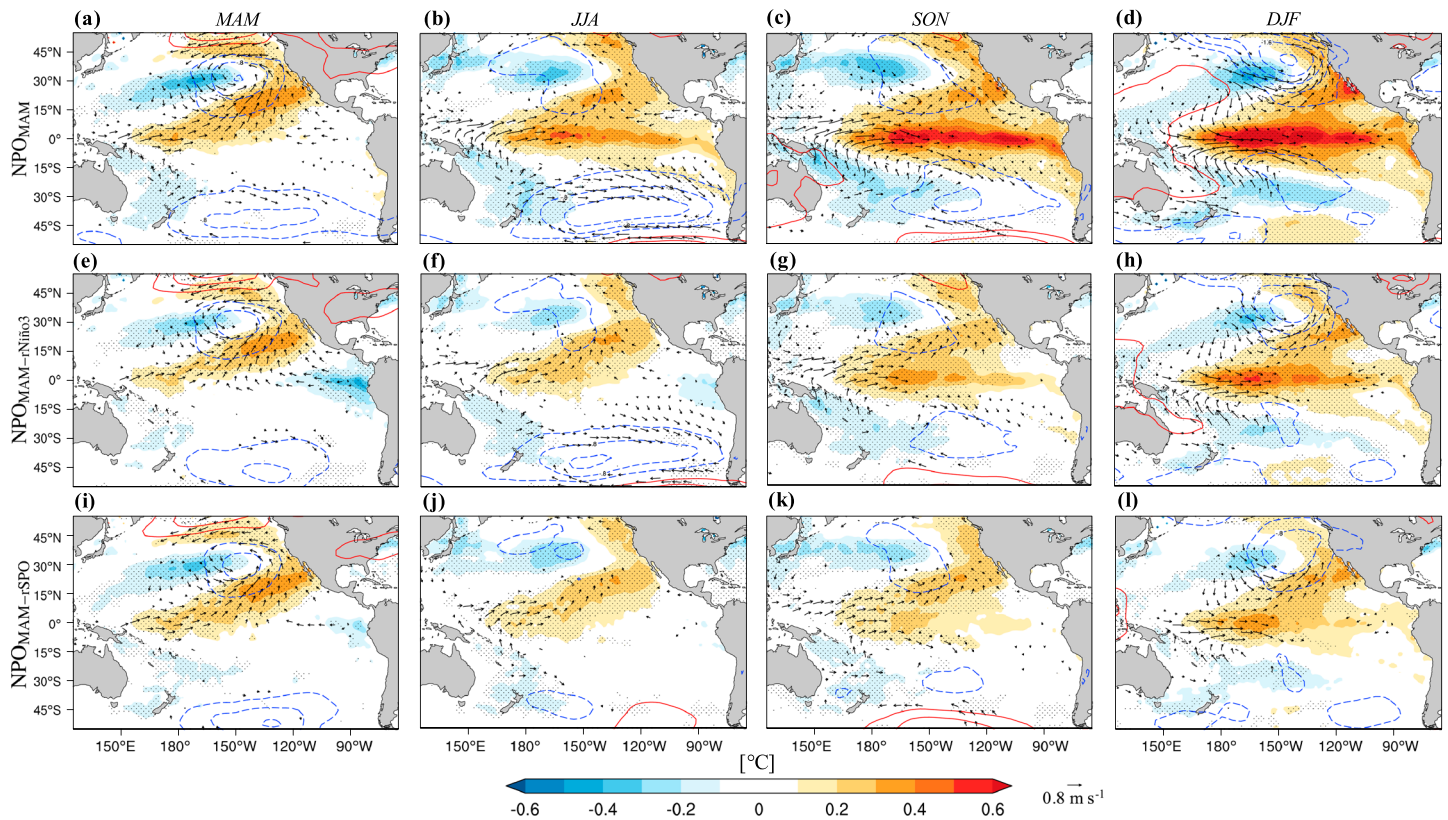


**Figure 4.** (a–d) As in Figures 2a–2d except for regressions onto the standardized  $\text{NPO}_{\text{MAM}}$  index. (e–h) As in Figures 4a–4d except for regressions onto the standardized  $\text{NPO}_{\text{MAM}-\text{rNiño}3}$  (see text for details). (i–l) As in Figures 4a–fig4d except for regressions onto the standardized  $\text{NPO}_{\text{MAM}-\text{rSPO}}$  (see text for details). Contour interval  $0.1^{\circ}\text{C}$  (shaded contours) and  $0.4 \text{ hPa}$  (line contours). Reference wind vector  $0.8 \text{ m s}^{-1}$ . Solid (dashed) line contours indicate positive (negative) values. Zero contour omitted. Stippling as in Figure 2.

We now examine how important the  $\text{SPO}_{\text{JJA}}$  variability is relative to the austral fall (boreal spring) NPO ( $\text{NPO}_{\text{MAM}}$ ) in the development of an ENSO event. The NPO index is traditionally defined as the second leading EOF of SLPa poleward of  $15^{\circ}\text{N}$  in the North Pacific [e.g., *Linkin and Nigam*, 2008]. However, it is the Hawaiian node that is most important for seasonal (and longer) linkages to the tropical Pacific [e.g., *Vimont et al.*, 2003; *Anderson*, 2003, 2007; *Di Lorenzo et al.*, 2010; *Furtado et al.*, 2012]. Therefore, for this study, we define the NPO index as the SLPa averaged over  $13^{\circ}\text{N}$ – $24^{\circ}\text{N}$  and  $158^{\circ}\text{W}$ – $135^{\circ}\text{W}$ . Figure 4 shows the lag regression of SLPa (line contours), SSTa (shading), and 10 m wind anomalies (vectors) onto three different indices:

1. The  $\text{NPO}_{\text{MAM}}$  index (Figures 4a–4d)
2. The  $\text{NPO}_{\text{MAM}-\text{rNiño}3}$  index, found by linearly removing the  $\text{Niño-3}_{\text{JJA}}$  index from  $\text{NPO}_{\text{MAM}}$  index:  $\text{NPO}_{\text{MAM}-\text{rNiño}3} = \text{NPO}_{\text{MAM}} - [\alpha_1 + \beta_1 \times \text{Niño3}_{\text{JJA}}]$  (Figures 4e–4h)
3. The  $\text{NPO}_{\text{MAM}-\text{rSPO}}$  index, found by linearly removing the  $\text{SPO}_{\text{JJA}}$  index from the  $\text{NPO}_{\text{MAM}}$  index:  $\text{NPO}_{\text{MAM}-\text{rSPO}} = \text{NPO}_{\text{MAM}} - [\alpha_2 + \beta_2 \times \text{SPO}_{\text{JJA}}]$  (Figures 4i–4l)

Figures 4a–4d show the ENSO life cycle as expected from the seasonal forecasting mechanism framework [e.g., *Vimont et al.*, 2003; *Chiang and Vimont*, 2004; *Chang et al.*, 2007]: the SSTa and wind anomalies extend from the subtropical North Pacific into the central and western tropical Pacific during MAM (Figure 4a). The SSTa subsequently expand into the eastern tropical Pacific and mature during DJF (Figures 4b–4d). When examining lag regressions of the same fields onto the  $\text{NPO}_{\text{MAM}-\text{rNiño}3}$  index (Figures 4e–4h), we see that, by construction, the tropical Pacific SSTa does not expand into the  $\text{Niño-3}$  region during JJA (Figure 4f). Nonetheless, a sizeable warming of the eastern tropical Pacific results during DJF (Figures 4g and 4h). This finding suggests that JJA  $\text{Niño-3}$  region positive SSTa are not necessary to result in an EP-type ENSO event (Figure 4d). Upon removing  $\text{SPO}_{\text{JJA}}$  variability from the  $\text{NPO}_{\text{MAM}}$  (Figures 4i–4l), the positive SSTa is now confined to the central equatorial Pacific throughout the period and develop in situ into a CP ENSO event, resembling the evolution shown by *Kug et al.* [2009] and *Kao and Yu* [2009]. Similar conclusions are found when examining ocean heat content

**Table 1.** All Major El Niño Events (23 Events, First Column), Their Types (Second Column; See Text for Definition), and Their Types Predicted by SPO (Third Column)<sup>a</sup>

Year	Type	Predicted by SPO <sub>JJA</sub>	Year	Type	Predicted by SPO <sub>JJA</sub>
1951	EP	✓	1987	EP	✓
1957	EP	✓	1990	CP	✓
1963	EP	✗	1991	EP	✗
1965	EP	✓	1994	CP	✓
1968	CP	✓	1997	EP	✓
1969	EP	✗	2002	CP	✗
1972	EP	✓	2004	CP	✓
1976	EP	✗	2006	EP	✓
1977	CP	✓	2009	CP	✓
1979	EP	✓	2014	CP	✓
1982	EP	✓	2015	EP	✗
1986	EP	✓		Total	17/23 = 74%

<sup>a</sup>Specifically, when the SPO<sub>JJA</sub> index is greater (less) than  $1\sigma$ , then an EP (a CP) El Niño is predicted.

anomalies (Figure S1 in the supporting information, line contours). Note that while these lag regression analyses cannot prove definitively the exact influence of the SPO on ENSO, they provide clues as to its contribution relative to the current paradigm involving the NPO.

### 3.3. The JJA SPO as a Potential Predictor for Different Types of ENSO

Given the previous results, the presence of the SPO signature in JJA may offer a plausible pathway to improve predictions of subsequent ENSO development and particularly the “flavor” of ENSO with  $\sim 6$  month lead. To test this assertion, we conduct a simple prediction exercise. For all El Niño events since 1948, the strength and phase of the SPO<sub>JJA</sub> index is used to predict if an EP or CP event would ensue. That is, if the SPO<sub>JJA</sub> index is greater (less) than  $1\sigma$ , an EP (a CP)-type event is predicted. The verification for our prediction follows the characterization of ENSO events as in Yeh *et al.* [2009], though the overall results are insensitive to other designations [e.g., Yu *et al.*, 2012]. Table 1 indicates that our simple prediction scheme identifies correctly the flavor of 74% (17 out of 23) of all observed El Niño events since 1948. This finding suggests that the SPO is a reliable (but not absolute) predictor for the type of ENSO event that will ensue with a 3–6 month lead.

Aside from identifying the flavor of warm ENSO events, the SPO may also play a role for La Niña events and the observed spatial asymmetries between El Niño and La Niña events. To examine this, we compute the asymmetric pattern between El Niño and La Niña [e.g., Larkin and Harrison, 2002; Anderson *et al.*, 2013b], i.e., the composite difference between SSTa during El Niño events and the inverse(i.e., multiplied by  $-1$ ) of SSTa during La Niña events. Figure 5 shows the results of the composite differences for all events (Figure 5a) and events conditioned by the phase and strength of the SPO (Figures 5b and 5c). When examining all events, the spatial difference in SSTa is minimal and statistically insignificant (Figure 5a). But when we examine the composite difference for events where magnitude of the SPO<sub>JJA</sub> is greater than  $1\sigma$ , the asymmetry between El Niño and La Niña is clearly visible with statistically significant differences in the easternmost tropical Pacific and near the dateline (Figure 5b, stippling). For cases when the magnitude of the SPO is less than  $1\sigma$ , the spatial patterns of the El Niño and La Niña SSTa match fairly well (i.e., small differences) with significant differences restricted to the far eastern tropical Pacific (Figure 5c). Hence, along with being a potential discriminant for the flavor of a warm ENSO event, the SPO may also play a role in the asymmetrical structure of warm and cold ENSO events like its northern counterpart the NPO [Anderson *et al.*, 2013b].

## 4. Summary and Discussion

Using reanalysis data, we demonstrated that South Pacific atmospheric variability associated with the South Pacific Oscillation (SPO) contributes significantly to the formation of ENSO events, particularly eastern Pacific (EP) ENSO events. The SPO is an inherent mode of variability with a contribution to its variability from the tropical Pacific SSTa (Figure 3). Through modulation of the climatological southeasterly trade winds, the positive phase of the SPO promotes anomalous equatorward ocean mass transport in the eastern equatorial Pacific, facilitating the growth of warm SSTa there and thus promoting EP-type ENSO events (Figures 2 and 4).

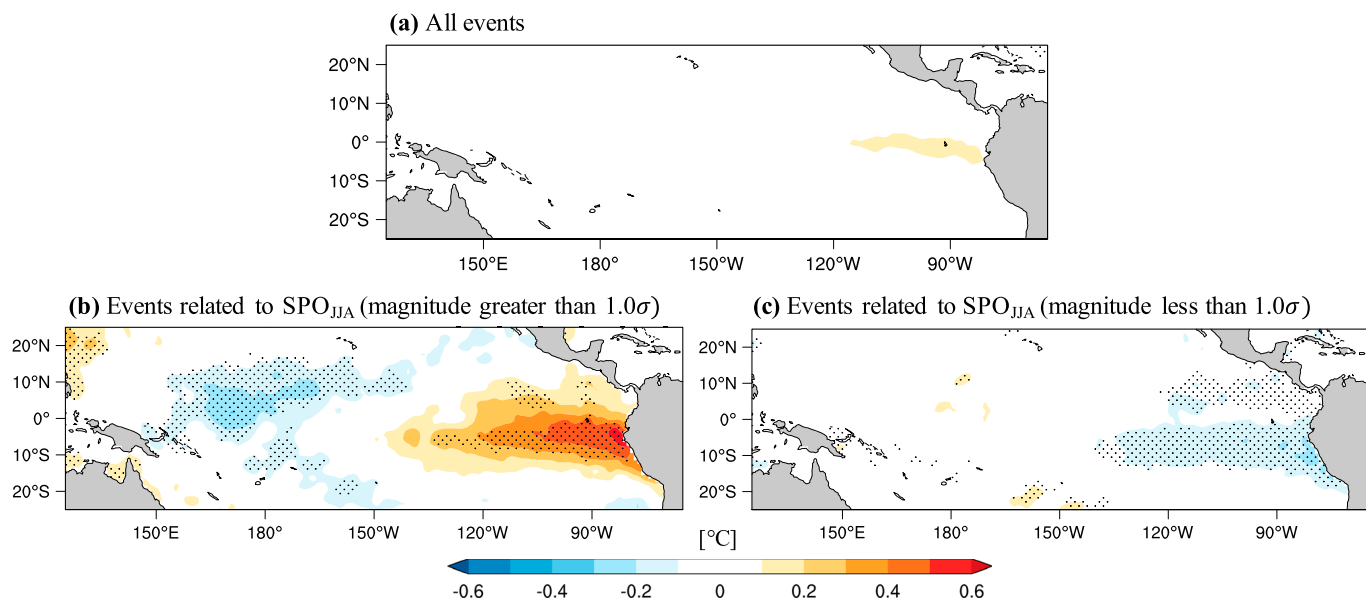


**Figure 5.** (a) Difference between the DJF-mean SSTa ( $^{\circ}$ C) for all El Niño events and the inverted DJF-mean (i.e., multiplied by  $-1$ ) for all La Niña events. (b) As in Figure 5a but only for El Niño (La Niña) events when the  $SPO_{JJA} \geq 1\sigma$  ( $SPO_{JJA} \leq -1\sigma$ ). (c) As in Figure 5a but for El Niño and La Niña events when  $|SPO_{JJA}| < 1\sigma$ . Contour interval  $0.1^{\circ}$ C. Stippling indicates composite differences that are significantly different from each other at the  $p < 0.05$  level according to a two-tailed Student's  $t$  test.

Our results also indicate that the SPO<sub>JJA</sub> is weaker prior to the maturation of CP events (Table 1), thus providing a potential enhancement to ENSO flavor prediction [e.g., Imada *et al.*, 2015].

With these results in mind, we now comment on how the SPO may have played a role in a poorly predicted ENSO event of 2014–2015. During 2014, the springtime North Pacific Oscillation (NPO) index reached a record-high positive value, and large positive SSTa extended from the subtropics into the central tropical Pacific region. Combined with dynamical model predictions, signs pointed to a strong El Niño event unfolding and maturing the following winter. However, this event did not develop as expected. Using our SPO framework, we offer one possible explanation for this “false alarm.” During JJA 2014, no strongly positive SPO signal was detected, unlike conditions prior to the previous strong events in 1982 and 1997 (Figure S2). Instead, anomalous *anticyclonic* flow dominated the South Pacific subtropics, *strengthening* the trade winds and likely triggering easterly wind bursts (Figure S2, right column) [see also Hu and Fedorov, 2016; Levine and McPhaden, 2016]. This negative phase of the SPO likely prevented the warm waters in the central tropical Pacific from propagating eastward, resulting in a more CP-like ENSO event (as predicted successfully with our framework—Table 1). Note that several other mechanisms have also been proposed to explain this nonevent [Min *et al.*, 2015; Imada *et al.*, 2016; Hu and Fedorov, 2016; Levine and McPhaden, 2016], but the SPO may also be another reason. Furthermore, the SPO was a *poor* predictor for the resulting strong EP event in 2015 (Table 1), highlighting its limitations.

The main focus for this paper has been on the SPO and its role in subseasonal and seasonal ENSO predictability. However, like the NPO, the subtropical node of the SPO too has significant quasi-decadal power and may therefore influence decadal tropical Pacific variability (Figures 1c and S3). This element of SPO variability may also impact the decadal modulation of ENSO asymmetry (Figure 5) and merits further investigation. Moreover, while our study highlights the SPO and its role in ENSO development and flavors, other processes like westerly wind bursts [Chen *et al.*, 2015], warm water volume precursors [Meinen and McPhaden, 2000], and other coupled atmosphere-ocean mechanisms [Zhang *et al.*, 2014] are also potential factors. Whether these processes work independently of or in concert with the SPO warrants research.

#### Acknowledgments

The authors would like to thank the various research groups and agencies for producing the necessary reanalysis data used in this study. The data used are freely accessible and available online at (1) NCEP/NCAR (<https://www.esrl.noaa.gov/psd/data/gridded/data.ncep.reanalysis.html>); (2) Met Office Hadley Center (<http://www.metoffice.gov.uk/hadobs/hadisst/>), and (3) ECMWF (<http://www.ecmwf.int/en/research/climate-reanalysis/ocean-reanalysis>). References to the reanalysis products are also included in the references list. The authors would also like to thank two anonymous reviewers for their insight and suggestions on improving the manuscript.

#### References

- Anderson, B. T. (2003), Tropical Pacific sea-surface temperatures and preceding sea level pressure anomalies in the subtropical North Pacific, *J. Geophys. Res.*, 108, 4732, doi:10.1029/2003JD003805.
- Anderson, B. T. (2007), Intraseasonal atmospheric variability in the extratropics and its relation to the onset of tropical Pacific sea surface temperature anomalies, *J. Clim.*, 20, 926–936.

- Anderson, B. T., and R. C. Perez (2015), ENSO and non-ENSO induced charging and discharging of the equatorial Pacific, *Clim. Dyn.*, 45(9), 2309–2327, doi:10.1007/s00382-015-2472-x.
- Anderson, B. T., R. C. Perez, and A. Karspeck (2013a), Triggering of El Niño onset through trade wind-induced charging of the equatorial Pacific, *Geophys. Res. Lett.*, 40(6), 1212–1216, doi:10.1002/grl.50200.
- Anderson, B. T., J. C. Furtado, K. M. Cobb, and E. Di Lorenzo (2013b), Extratropical forcing of El Niño–Southern Oscillation asymmetry, *Geophys. Res. Lett.*, 40(18), 4916–4921, doi:10.1002/grl.50951.
- Ashok, K., S. K. Behera, S. A. Rao, H. Weng, and T. Yamagata (2007), El Niño Modoki and its possible teleconnection, *J. Geophys. Res. Oceans*, 112, C11007, doi:10.1029/2006JC003798.
- Balmaseda, M. A., K. Mogensen, and A. T. Weaver (2013), Evaluation of the ECMWF ocean reanalysis system ORAS4, *Q. J. R. Meteorol. Soc.*, 139(674), 1132–1161, doi:10.1002/qj.2063.
- Bretherton, C. S., M. Widmann, V. P. Dymnikov, J. M. Wallace, and I. Bladé (1999), The effective number of spatial degrees of freedom of a time-varying field, *J. Clim.*, 12(7), 1990–2009.
- Capotondi, A., et al. (2015), Understanding ENSO diversity, *Bull. Am. Meteorol. Soc.*, 96(6), 921–938, doi:10.1175/BAMS-D-13-00117.1.
- Chang, P., L. Zhang, R. Saravanan, D. J. Vimont, J. C. H. Chiang, L. Ji, H. Seidel, and M. K. Tippett (2007), Pacific meridional mode and El Niño–Southern Oscillation, *Geophys. Res. Lett.*, 34, L16608, doi:10.1029/2007GL030302.
- Chen, D., T. Lian, C. Fu, M. A. Cane, Y. Tang, R. Murtugudde, X. Song, Q. Wu, and L. Zhou (2015), Strong influence of westerly wind bursts on El Niño diversity, *Nat. Geosci.*, 8(5), 339–345.
- Chiang, J. C. H., and D. J. Vimont (2004), Analogous Pacific and Atlantic meridional modes of tropical atmosphere-ocean variability, *J. Clim.*, 17(21), 4143–4158, doi:10.1175/JCLI4953.1.
- Di Lorenzo, E., K. M. Cobb, J. C. Furtado, N. Schneider, B. T. Anderson, A. Bracco, M. A. Alexander, and D. J. Vimont (2010), Central Pacific El Niño and decadal climate change in the North Pacific, *Nat. Geosci.*, 3, 762–765.
- Di Lorenzo, E., G. Ligueri, N. Schneider, J. C. Furtado, B. T. Anderson, and M. A. Alexander (2015), ENSO and meridional modes: A null hypothesis for Pacific climate variability, *Geophys. Res. Lett.*, 42, 9440–9448, doi:10.1002/2015GL066281.
- Ding, R., J. Li, Y.-h. Tseng, C. Sun, and Y. Guo (2015), The Victoria mode in the North Pacific linking extratropical sea level pressure variations to ENSO, *J. Geophys. Res. Atmos.*, 120, 27–45, doi:10.1002/2014JD022221.
- Furtado, J. C., E. Di Lorenzo, B. T. Anderson, and N. Schneider (2012), Linkages between the North Pacific Oscillation and central tropical Pacific SSTs at low frequencies, *Clim. Dyn.*, 39(12), 2833–2846, doi:10.1007/s00382-011-1245-4.
- Hu, S., and A. V. Fedorov (2016), Exceptionally strong easterly wind burst stalling El Niño of 2014, *Proc. Natl. Acad. Sci. U.S.A.*, 113(8), 2005–2010.
- Imada, Y., H. Tatebe, M. Ishii, Y. Chikamoto, M. Mori, M. Arai, M. Watanabe, and M. Kimoto (2015), Predictability of two types of El Niño assessed using an extended seasonal prediction system by MIROC, *Mon. Weather Rev.*, 143(11), 4597–4617, doi:10.1175/MWR-D-15-0007.1.
- Imada, Y., H. Tatebe, M. Watanabe, M. Ishii, and M. Kimoto (2016), South Pacific influence on the termination of El Niño in 2014, *Sci. Rep.*, 6, 30341.
- Jin, D., and B. P. Kirtman (2009), Why the Southern Hemisphere ENSO responses lead ENSO, *J. Geophys. Res. Atmos.*, 114, D23101, doi:10.1029/2009JD012657.
- Jin, F.-F. (1997), An equatorial ocean recharge paradigm for ENSO. Part I: Conceptual model, *J. Atmos. Sci.*, 54, 811–829, doi:10.1175/1520-0469(1997)054<0811:AEORPF>2.0.CO;2.
- Johnson, N. C. (2013), How many ENSO flavors can we distinguish?, *J. Clim.*, 26(13), 4816–4827, doi:10.1175/JCLI-D-12-00649.1.
- Kalnay, E., et al. (1996), The NCEP/NCAR 40-year reanalysis project, *Bull. Am. Meteorol. Soc.*, 77(3), 437–471.
- Kao, H.-Y., and J.-Y. Yu (2009), Contrasting eastern-Pacific and central-Pacific types of ENSO, *J. Clim.*, 22(3), 615–632, doi:10.1175/2008JCLI2309.1.
- Karnauskas, K. B. (2013), Can we distinguish canonical El Niño from Modoki?, *Geophys. Res. Lett.*, 40, 5246–5251, doi:10.1002/grl.51007.
- Kug, J.-S., F.-F. Jin, and S.-I. An (2009), Two types of El Niño events: Cold tongue El Niño and warm pool El Niño, *J. Clim.*, 22(6), 1499–1515, doi:10.1175/2008JCLI2624.1.
- Larkin, N. K., and D. E. Harrison (2002), ENSO warm (El Niño) and cold (La Niña) event life cycles: Ocean surface anomaly patterns, their symmetries, asymmetries, and implications, *J. Clim.*, 15, 1118–1139.
- Levine, A. F. Z., and M. J. McPhaden (2016), How the July 2014 easterly wind burst gave the 2015–2016 El Niño a head start, *Geophys. Res. Lett.*, 43, 6503–6510, doi:10.1002/2016GL069204.
- Linkin, M. E., and S. Nigam (2008), The North Pacific Oscillation-West Pacific Teleconnection Pattern: Mature-phase structure and winter impacts, *J. Clim.*, 21(9), 1979–1997, doi:10.1175/2007JCLI2048.1.
- McGregor, S., N. J. Holbrook, and S. B. Power (2009a), The response of a stochastically forced ENSO model to observed off-equatorial wind stress forcing, *J. Clim.*, 22(10), 2512–2525, doi:10.1175/2008JCLI2387.1.
- McGregor, S., A. S. Gupta, N. J. Holbrook, and S. B. Power (2009b), The modulation of ENSO variability in CCSM3 by extratropical Rossby waves, *J. Clim.*, 22(22), 5839–5853, doi:10.1175/2009JCLI2922.1.
- Meinen, C. S., and M. J. McPhaden (2000), Observations of warm water volume changes in the equatorial pacific and their relationship to El Niño and La Niña, *J. Clim.*, 13(20), 3551–3559.
- Min, Q., J. Su, R. Zhang, and X. Rong (2015), What hindered the El Niño pattern in 2014?, *Geophys. Res. Lett.*, 42, 6762–6770, doi:10.1002/2015GL064899.
- North, G. R., T. L. Bell, R. F. Cahalan, and F. J. Moeng (1982), Sampling errors in the estimation of empirical orthogonal functions, *Mon. Weather Rev.*, 110(7), 699–706.
- Rasmusson, E. M., and T. H. Carpenter (1982), Variations in tropical sea surface temperature and surface wind fields associated with the Southern Oscillation/El Niño, *Mon. Weather Rev.*, 110(5), 354–384.
- Rayner, N. A., D. E. Parker, E. B. Horton, C. K. Folland, L. V. Alexander, D. P. Rowell, E. C. Kent, and A. Kaplan (2003), Global analyses of sea surface temperature, sea ice, and night marine air temperature since the late nineteenth century, *J. Geophys. Res.*, 108(D14), 4407, doi:10.1029/2002JD002670.
- Rogers, J. C. (1981), The North Pacific Oscillation, *J. Clim.*, 1(1), 39–57, doi:10.1002/joc.3370010106.
- Suarez, M. J., and P. S. Schopf (1988), A delayed action oscillator for ENSO, *J. Atmos. Sci.*, 45, 3283–3287, doi:10.1175/1520-0469(1988)045<3283:ADAOFE>2.0.CO;2.
- Vimont, D. J., J. M. Wallace, and D. S. Battisti (2003), The seasonal footprinting mechanism in the Pacific: Implications for ENSO, *J. Clim.*, 16(16), 2668–2675.
- Wyrtki, K. (1975), El Niño—The dynamic response of the Equatorial Pacific Ocean to atmospheric forcing, *J. Phys. Oceanogr.*, 5, 572–584.
- Yeh, S.-W., J.-S. Kug, B. Dewitte, M.-H. Kwon, B. P. Kirtman, and F.-F. Jin (2009), El Niño in a changing climate, *Nature*, 461(7263), 511–514.

- Yu, J.-Y., H.-Y. Kao, and T. Lee (2010), Subtropics-related interannual sea surface temperature variability in the central equatorial Pacific, *J. Clim.*, 23(11), 2869–2884, doi:10.1175/2010JCLI3171.1.
- Yu, J.-Y., Y. Zou, S. T. Kim, and T. Lee (2012), The changing impact of El Niño on US winter temperatures, *Geophys. Res. Lett.*, 39, L15702, doi:10.1029/2012GL052483.
- Zhang, H., A. Clement, and P. D. Nezio (2014), The South Pacific meridional mode: A mechanism for ENSO-like variability, *J. Clim.*, 27(2), 769–783, doi:10.1175/JCLI-D-13-00082.1.